Investigation of temperature influence on output performance of high-power cladding-pumped Er,Yb co-doped fiber laser

Wenting Chen, Jianjian Sha, Yong Wang, Deyuan Shen*
Key laboratory of Micro and Nano Photonic Structures (Ministry of Education), Department of Optical Science and Engineering, Fudan University, Shanghai 200433, China

ABSTRACT

Effect of the fiber's temperature on lasing performance is investigated in high-power, cladding-pumped Er, Yb co-doped fiber laser system. A three-layer symmetric cylindrical model is applied to describe the temperature distribution of the fiber under natural air convection. Radial temperature distribution of the fiber is calculated with consideration of the quantum defect heat, the heat from the absorption of spontaneous emission, and the convection and radiation at the heat transfer boundaries. The steady-state theoretical model based on rate equations takes into account of the energy transfers between Er^{3+}-ions and Yb^{3+}-ions and a fraction of nonparticipatory Yb^{3+}-ions. Shooting method and Newton iteration method are used to solve the boundary-value problems under different environmental temperatures, pump powers and reflectivities at the fiber ends. Numerical simulations are consistent with experimental results and show that increasing the fiber's temperature is an effective strategy to suppress the 1 μm parasitic lasing and improve the lasing performance at 1.5 μm, a similar phenomenon is found with enhancing doping concentrations of the two ions and decreasing the reflectivities at the fiber ends. Our numerical results present a theoretical guideline for further improving the laser performance in terms of output power of ~1.5 μm in high-power Er,Yb-doped fiber laser systems.

Keywords: cladding-pumped, Er, Yb co-doped fiber laser, thermal effects, modeling

1. INTRODUCTION

High-power double-clad fiber lasers at the eye-safe 1.5 μm wavelength range have attracted a lot of interests owing to their high brightness, good beam quality, outstanding thermal handling capability and widely practical applications. They have successfully found their positions in fields such as optical communication, medical imaging, machine welding and military industry. Double-clad fibers with Er^{3+}-ions doping are usually used to construct lasers operating at 1.5 μm region. The Er^{3+}-ions single-doped fiber lasers suffer from low efficiency due to low pumping absorption and severe clustering effects. Generally, co-doping with Yb^{3+}-ions is considered as a useful method to increase the 1.5 μm output efficiency[1]. But this also brings the unwanted 1 μm parasitic lasing and heat generated by the large quantum defect. In this paper, we investigate the environmental temperature's influence on the output performance of Er,Yb co-doped fiber laser systems exploring the relation between 1 μm parasitic lasing and 1.5 μm lasing by building a numerical model considering the heat generated in the core. Fiber doping concentrations and reflections at fiber ends' influences are also discussed.

*shendy@fudan.edu.cn

Fiber Lasers X: Technology, Systems, and Applications, edited by Sami T. Hendow, Proc. of SPIE
Vol. 8601, 86012A · © 2013 SPIE · CCC code: 0277-786X/13/$18 · doi: 10.1117/12.2002720

2. ERBIUM YTTERBIUM CODEPED FIBER LASER MODEL

2.1. Fiber laser model

We present a model describing a fiber laser of length L. Its effective feedback of the lasing resonator is all provided by the Fresnel reflections (R_1, R_2) at fiber ends (Z=0, Z=L). Figure 1 shows the energy level diagram of Er,Yb co-doped fiber laser system. Pump power are absorbed by Er^{3+}-ions and Yb^{3+}-ions in the ground state and excited to the $^4I_{11/2}$ and $^2F_{5/2}$ level. Excited Yb^{3+}-ions transfer energy to Er^{3+}-ions in the $^4I_{11/2}$ level and back transfer also happens. The excited Er^{3+}-ions relax very quickly to the $^4I_{13/2}$ level thus reduce the back transfer from Er^{3+}-ions to Yb^{3+}-ions. Laser transitions at 1.5 μm occur between level $^4I_{13/2}$ and $^4I_{15/2}$. Cooperative energy transfer between $^4I_{9/2}$, $^4I_{13/2}$ and $^4I_{15/2}$ is considered. It is assumed that Er^{3+}-ions in the $^4I_{9/2}$ level decay instantaneously to the $^4I_{11/2}$ level implying $N_4 \approx 0$. We also take into account that a fraction of Yb^{3+}-ions does not participate in energy exchange with Er^{3+}-ions[2].

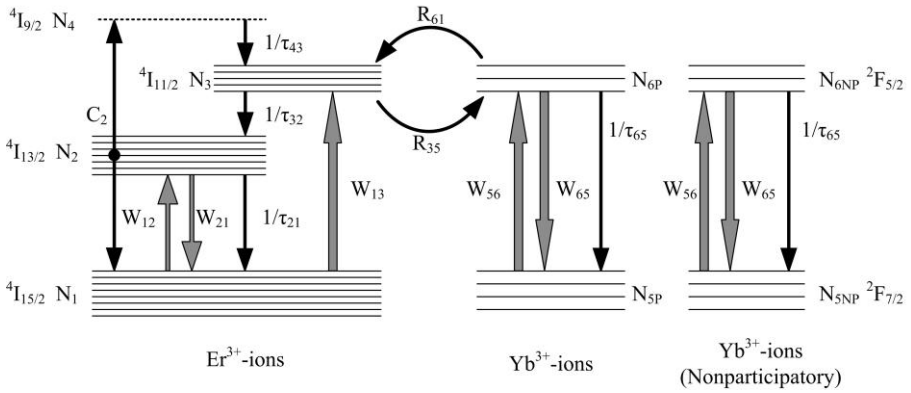

Figure 1. Energy level diagram for the Er,Yb co-doped systems.

The rate equations and power propagation equations describing the Er,Yb co-doped fiber laser systems can be expressed as follows:

$$\frac{\partial N_2}{\partial t} = -\frac{N_2}{\tau_{21}} + \frac{N_3}{\tau_{32}} + W_{12}N_1 - W_{21}N_2 - 2C_2N_2^2 \tag{1}$$

$$\frac{\partial N_3}{\partial t} = -\frac{N_3}{\tau_{32}} + W_{13}N_1 + C_2N_2^2 + R_{61}N_{6P}N_1 - R_{35}N_3N_{5P} \tag{2}$$

$$\frac{\partial N_{6P}}{\partial t} = -\frac{N_{6P}}{\tau_{65}} + W_{56}N_{5P} - W_{65}N_{6P} - R_{61}N_{6P}N_1 + R_{35}N_3N_{5P} \tag{3}$$

$$\frac{\partial N_{6NP}}{\partial t} = -\frac{N_{6NP}}{\tau_{65}} + W_{56}N_{5NP} - W_{65}N_{6NP} \tag{4}$$

$$N_5 = N_{5P} + N_{5NP} \tag{5}$$

$$N_6 = N_{6P} + N_{6NP} \tag{6}$$

$$N_{\mathrm{Yb}} = N_5 + N_6 \tag{7}$$

$$N_{Er} = N_1 + N_2 + N_3 \tag{8}$$

$$\pm\frac{dP_{Er}^{\pm}(z)}{dz} = \left\{\Gamma(\lambda_{s1})\left[N_2\sigma_{21}(\lambda_{s1}) - N_1\sigma_{12}(\lambda_{s1})\right] - \alpha(\lambda_{s1})\right\}P_{Er}^{\pm}(z) + \frac{2hc^2}{\lambda_{s1}^3}\Gamma(\lambda_{s1})N_2\sigma_{21}(\lambda_{s1})m_s\Delta\lambda \tag{9}$$

$$\pm\frac{dP_{Yb}^{\pm}(z)}{dz}=\left\{\Gamma(\lambda_{s2})\left[N_6\sigma_{65}(\lambda_{s2})-N_5\sigma_{56}(\lambda_{s2})\right]-\alpha(\lambda_{s2})\right\}P_{Yb}^{\pm}(z)+\frac{2hc^2}{\lambda_{s2}^3}\Gamma(\lambda_{s2})N_6\sigma_{65}(\lambda_{s2})m_p\Delta\lambda \tag{10}$$

$$\pm\frac{dP_{p}^{\pm}(z)}{dz}=\left\{\Gamma(\lambda_{p})\left[N_6\sigma_{65}(\lambda_{p})-N_5\sigma_{56}(\lambda_{p})\right]-\alpha(\lambda_{p})\right\}P_{p}^{\pm}(z) \tag{11}$$

where N_{Er} and N_{Yb} are Er^{3+}-ions and Yb^{3+}-ions concentrations; N_1, N_2, N_3, N_4, N_5 and N_6 are annotated in Fig. 1. λ_p is the pump wavelength at 975 nm, λ_{s1} is the Er^{3+}-ions lasing wavelength at 1550 nm, λ_{s2} is the Yb^{3+}-ions parasitic lasing wavelength at 1064 nm. $P_p^{\pm}(z)$, $P_{Er}^{\pm}(z)$, $P_{Yb}^{\pm}(z)$ are the pump, 1.5 μm output and 1 μm output power in the forward (+) and backward (-) directions. τ_{ij} terms are the relaxation lifetimes. $\sigma_{ij}(\lambda)$ terms are absorption and emission cross sections. R_{61} and R_{35} are the energy transfer coefficients between the $^4I_{11/2}$ and $^2F_{5/2}$ level. C_2 is the up-conversion coefficient. The value of energy transfer coefficient and up-conversion coefficient are linear functions of Yb^{3+}-ions and Er^{3+}-ions concentrations respectively [3]. $\alpha(\lambda)$ is the fiber attenuation coefficient, representing scattering loss. h is the Plank constant. c is the light velocity in the vacuum. $2hc^2/\lambda_k^3$ is the contribution of spontaneous emission into the propagation laser mode. m_s, m_p are effective numbers of spontaneous emission transverse modes. Signal bandwidth ($\Delta\lambda$) is considered to be 1 nm.

The stimulated pump and 1 μm output absorption and emission rates W_{56}, W_{65} and W_{13} are given by:

$$W_{ij}(z)=\frac{\Gamma_p\sigma_{ij}(\lambda_p)\left[P_p^{+}(z)+P_p^{-}(z)\right]\lambda_p}{hcA_{core}}+\frac{\Gamma(\lambda_{s2})\sigma_{ij}(\lambda)\left[P_{Yb}^{+}(z,\lambda_{s2})+P_{Yb}^{-}(z,\lambda_{s2})\right]\lambda_{s2}}{hcA_{core}} \tag{12}$$

The stimulated 1.5 μm output absorption and emission rates W_{12} and W_{21} are given by:

$$W_{lm}(z)=\frac{\Gamma(\lambda_{s1})\sigma_{lm}(\lambda_{s1})\left[P_{Er}^{+}(z,\lambda_{s1})+P_{Er}^{-}(z,\lambda_{s1})\right]\lambda_{s2}}{hcA_{core}} \tag{13}$$

where $\Gamma(\lambda)$ is a wavelength-dependent power overlap factor, whose expression and value is derived in Ref. [4]. A_{core} is the cross section area of core.

Power propagation equations (9) (10) (11) must satisfy boundary conditions expressed as following:

$$P^{+}(0,\lambda)=R_1(\lambda)P^{-}(0,\lambda) \tag{14}$$

$$P^{-}(L,\lambda)=R_2(\lambda)P^{+}(L,\lambda) \tag{15}$$

where we assume the fiber end facets are perpendicularly cleaved hence according to the Fresnel equations, $R_1(\lambda_{s1})=R_2(\lambda_{s1})\approx 0.036$; $R_1(\lambda_{s2})=R_2(\lambda_{s2})\approx 0.034$. Shooting method and Newton iteration method are used to solve the two-point boundary-value problems.

In our simulations, the fiber is assumed to be 5 m long with its core, inner cladding and outer cladding diameter to be 30 μm, 400 μm and 640 μm. Cross sections σ_{ij} are obtained from Ref. [4]. R_{61}, R_{35} and C_2 are calculated from Equation (15) in Ref. [3]. $m_s=2$, $m_p=4$ are used according to Ref. [4]. Other fiber parameters are listed in Table 1.

Table 1. Parameters used in the simulations.

Parameter	Value	Unites
N_{Er}	5.1×10^{25}	m^{-3}
N_{Yb}	7.6×10^{26}	m^{-3}
τ_{21}	10×10^{-3}	s
τ_{32}	1×10^{-7}	s
τ_{65}	1.3×10^{-3}	s
$\alpha(\lambda_{s1})$	3.2×10^{-3}	m^{-1}
$\alpha(\lambda_{s2})$	5×10^{-3}	m^{-1}
$\alpha(\lambda_{p})$	6.5×10^{-3}	m^{-1}

2.2. Three layer geometry

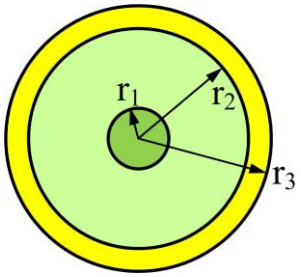

Figure 2. Cross-sectional geometry of the double cladding fiber. (r_1 is the radius of the doped core, r_2 is the radius of the inner silica cladding, r_3 is the radius of the outer polymer cladding)

We present a three-layer coaxial fiber geometrical model for describing the temperature distribution in the cross section direction of the double-clad fiber (as shown in Figure 2). Core and inner-cladding are silica, outer-cladding is polymer. The fiber is assumed to be under conventional air-cooling. Spontaneous emission absorption in the polymer coating [5] and radiation at the heat transfer boundary at $r = r_3$ are taken into account [6]. At high pump powers, radiation becomes important in the process of heat transfer as discussed in Ref. [6]. Heat generated in the core of the fiber per volume is estimated using $Q = P_{diss}/(L \cdot A_{core})$, where P_{diss} is the absorbed pump power minus the signal output power at 1.5 μm and 1 μm. The temperature distributions in the fiber laser are governed by the following steady-state heat conduction, convection and radiation equations in symmetric cylindrical coordinates:

$$\frac{1}{r}\frac{\partial}{\partial r}\left(r\frac{\partial T_1}{\partial r}\right)+\frac{Q}{k_s}=0\,,\ 0\le r\le r_1 \tag{16}$$

$$\frac{1}{r}\frac{\partial}{\partial r}\left(r\frac{\partial T_2}{\partial r}\right)=0\,,\ r_1\le r\le r_2 \tag{17}$$

$$\frac{1}{r}\frac{\partial}{\partial r}\left(r\frac{\partial T_3}{\partial r}\right)+\frac{\chi}{k_p}\frac{\exp(-\alpha r)}{r}=0\,,\ r_2\le r\le r_3 \tag{18}$$

where T_1, T_2 and T_3 represent the temperature in core, inner-cladding and outer-cladding of the fiber. k_s and k_p are the thermal conductivity of silica and polymer. α is the absorption coefficient in the wavelength range of spontaneous

emission in the polymer coating. $\chi = \alpha I_0 r_2 \exp(\alpha r_2)$, in which I_0 is the luminescence intensity at $r = r_2$. I_0 could be expressed as $I_0 = (1-\eta) P_p / (L \cdot 2\pi r_2)$, where η represents the fraction of pump power converted to heat.

The temperatures must be continuous across the boundary $r = r_1 / r_2 / r_3$. The derivatives of temperatures at boundary of the same materials must be continuous. The temperatures' derivatives at two different materials must be in inverse proportion to their thermal conductivities. At the boundary of polymer and air, Newton's law of cooling is assumed. So the multipoint boundary conditions of the thermal equations are given as follows:

$$T_1(r_1) = T_2(r_1) \tag{19}$$

$$T_2(r_2) = T_3(r_2) \tag{20}$$

$$\left.\frac{dT_1}{dr}\right|_{r_1=0} = 0 \tag{21}$$

$$\left.\frac{dT_1}{dr}\right|_{r_1} = \left.\frac{dT_2}{dr}\right|_{r_1} \tag{22}$$

$$k_s \left.\frac{dT_2}{dr}\right|_{r_2} = k_p \left.\frac{dT_3}{dr}\right|_{r_2} \tag{23}$$

$$\left.\frac{dT_3}{dr}\right|_{r_3} = \frac{H}{k_p}\left(T_{air} - T_3(r_3)\right) \tag{24}$$

where H is the total heat transfer: $H=h_c+h_r$; h_c is the convective heat-transfer coefficient; h_r is the radiative heat-transfer coefficient. h_c and h_r can be obtained from the following equations:

$$h_c = 0.5 N_u k_a r_3^{-1} \tag{25}$$

$$N_u \exp\left(-\frac{2}{N_u}\right) = 0.16\left(G_r P_r\right)^{\frac{1}{3}} \tag{26}$$

$$G_r = 8 g d_A^2 \mu_A^{-2} r_3^3 T_{air}^{-1} \left(T_3(r_3) - T_{air}\right) \tag{27}$$

$$h_r = \frac{\varepsilon \sigma_b \left(T_3^4(r_3) - T_{air}^4\right)}{T_3(r_3) - T_{air}} \tag{28}$$

N_u, G_r, P_r are the Nusselt, Grashof, and Prandtl numbers. g is the acceleration of gravity. d_A, μ_A and k_a are the density, viscosity and thermal conductivity of air. ε is the emissivity. σ_b is the Stefan-Boltzmann constant. At room temperature T_{air} =300 K, the following parameters are used: k_s =1.38 W • m^{-1} • K^{-1}, k_p =0.24 W • m^{-1} • K^{-1}, k_a =0.026 W • m^{-1} • K^{-1}, g =9.8 m • s^{-2}, P_r =0.71, d_A =1.2 kg • m^{-3}, μ_A =1.85×10^{-5} kg • m^{-1}, ε =0.85, σ_b =5.669×10^{-8} W • m^{-2} • K^4, α =10.

2.3. Temperature distributions in a double cladding fiber

Figure 3 shows the numerically calculated temperature profile in the radial direction of the fiber under double-end pumping power of 940 W. The fiber laser is assumed to operate under natural air-cooling in environmental (room) temperature of 300 K. The profile shows that heat generated in the fiber resulted in a temperature increase of the polymer cladding from 300K to 568 K, e.g. ~268 K increase. The temperature at the center of the core is 26 K higher than the outside boundary of the fiber, which is 594 K. In our modeling, we assume the temperature along the fiber is evenly distributed. While in fact, because the pump power and output power are stronger at fiber ends, the temperatures are higher at fiber ends.

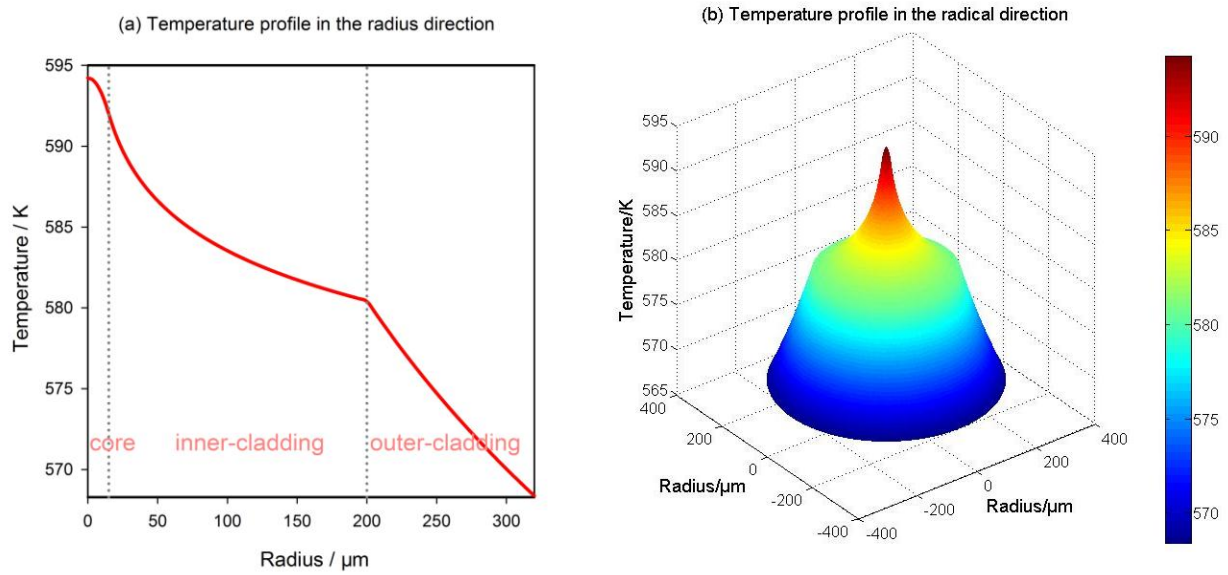

Figure 3. Temperature profile in the radial direction.

2.4. Effect of self-generated heat on the Stark population

Taking into consideration that the levels in each manifold are in thermal equilibrium, the relative Boltzmann distribution of Stark sublevels in each manifold at temperature T_{room} (room temperature, 300K) and T_{core} (central temperature of the fiber, 594 K) are shown in Fig. 4. It could be seen from Fig.4 that the population of Stark sublevels of Er^{3+}-ions are more evenly distributed. This could be attributed to the fact that the number of Stark sublevels of Er^{3+}-ions is almost twice as large as that of Yb^{3+}-ions. According to the definition of emission cross section (σ_e), the σ_e at core temperature T_{core} has a relationship with σ_e at room temperature (marked as T_{room}):

$$\sigma_e(\lambda, T_{core}) = \sigma_e(\lambda, T_r)\frac{Z_u(T_{room})}{Z_u(T_{core})} \tag{29}$$

where Z_u and Z_l represent the partition distribution functions of upper and lower energy level at temperature T which are defined as:

$$Z_i = \sum_i \exp\left(-\frac{\Delta E_i}{k_B T}\right) \tag{30}$$

where ΔE_i is the energy of i -th Stark level with respect to the bottom of this manifold, k_B is the Boltzmann constant. According to equations (29) and (30), we can get the conclusion that the cross sections of Yb^{3+}-ions are more sensitive to the change of temperature. Figure 5 shows the energy levels of Yb^{3+}-ions in silica with pump transition at 975 nm and output laser transition at 1064 nm labeled. As to the laser transition at 1064 nm from level e→c, its probability decreases along with rising of temperature because the population at upper level e decreases by 19% and at lower level c increases by 236% according to Fig.4 when the temperature increases from 300 K to 594 K.

With the calculated emission cross section value at T , the absorption cross section value at T could be obtained using the McCumber relation [7]:

$$\sigma_a = \sigma_e \frac{Z_u}{Z_l}\exp\left(-\frac{E_{ZL} - h\upsilon}{k_B T}\right) \tag{31}$$

where E_{ZL} is the energy gap between the bottom Stark sublevel in the upper and lower manifolds, e.g. Zero-line energy. υ is the laser frequency.

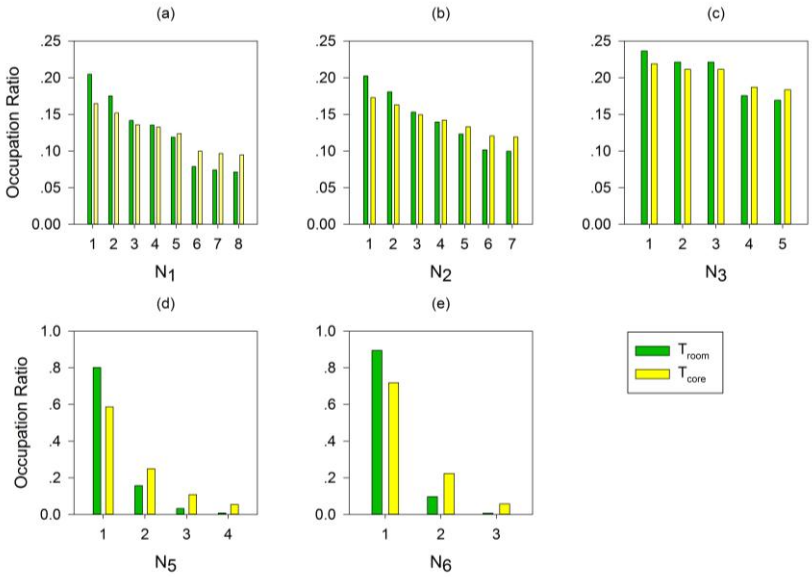

Figure 4. Relative population of the upper and lower Stark sublevels of Er^{3+}-ions and Yb^{3+}-ions for T_{room} =300 K and T_{core} =594 K.

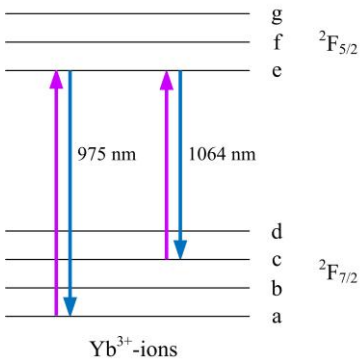

Figure 5. Energy levels of Yb^{3+}-ions in silica with pump and output laser transitions labeled.

2.5. Modeling output results

The values of pump power and output power at 1.5 μm and 1 μm along the 5-m long fiber are shown in Fig. 6. At room temperature of 273 K, under double-end pumping power of 940 W (with 470 W at each end), the total output power at 1.5 μm is 237 W, at 1 μm is 526 W. Almost all pump power is absorbed along the 5-m fiber. The overall conversion efficiency is 81%. It should be mentioned that both the pump power and output power reach maximum at fiber ends so in practice the temperature is not uniformly distributed along the fiber but gets maximum at fiber ends.

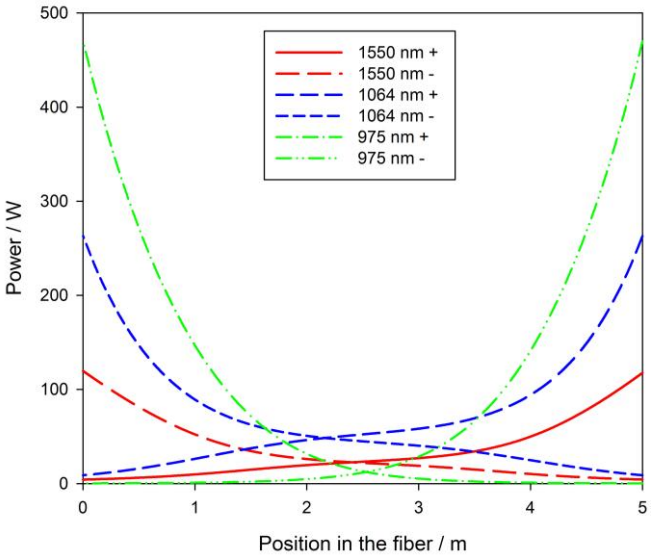

Figure 6. Pump and output power distribution as a function of position along the fiber for a total two-ends input pump power of 940 W, T_{room} =273 K at λ=975 nm.

Numerical results with and without temperature dependence are drawn and compared with experimental result in Ref. [8], which is also the highest reported 1.5 μm output experimental result in Er,Yb co-doped fiber laser system. It clearly shows that modeling result with temperature dependence is closer to the experimental result: the 1.5 μm output power saturates at higher pump powers and the 1 μm parasitic output increases slower while increasing the pump power. In our modeling, when the 1 μm output starts to oscillate, the 1.5 μm output starts to saturate; while this turning point is not so obvious in the experimental results. The discrepancy may be attributed to the different approximations made.

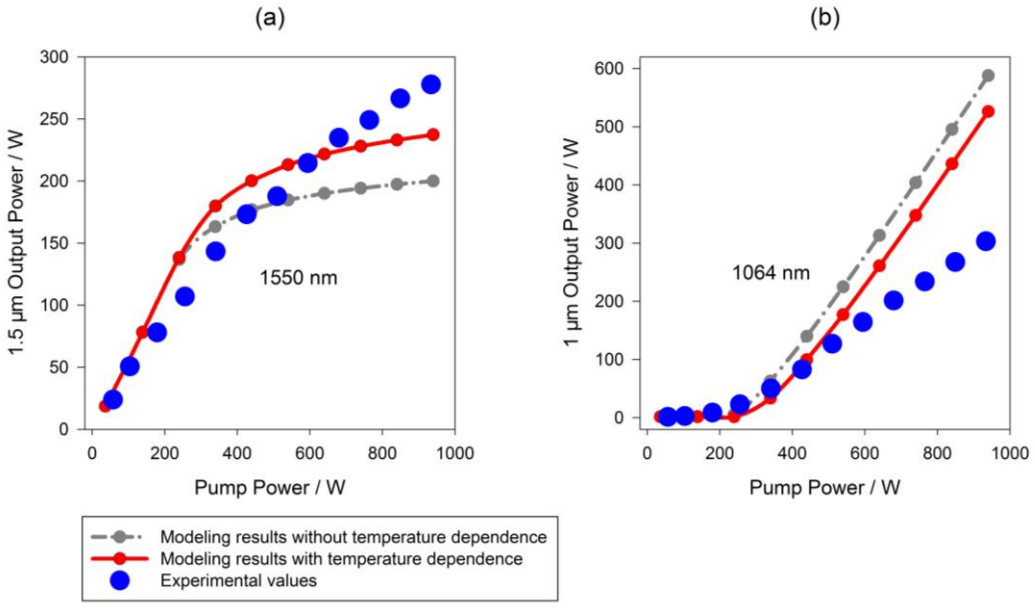

Figure 7. Comparison of experimental values at 1.5 μm and 1.0 μm with modeling results with and without temperature dependence: (a) 1.5 μm output (b) 1 μm output.

3. DISCUSSION

3.1. Temperature effects

Our calculations show that by increasing the environmental temperature of this Er,Yb co-doped fiber laser from 273 K to 373 K, the 1.5 μm output power increases while the 1 μm output power decreases. As expected, the output variation of the 1 μm lasing is larger with respect to the 1.5 μm lasing while enhancing the environmental temperature. We could conclude from Fig. 8 that increasing environmental temperature provides a method to improve the output performance of Er,Yb-doped fiber laser.

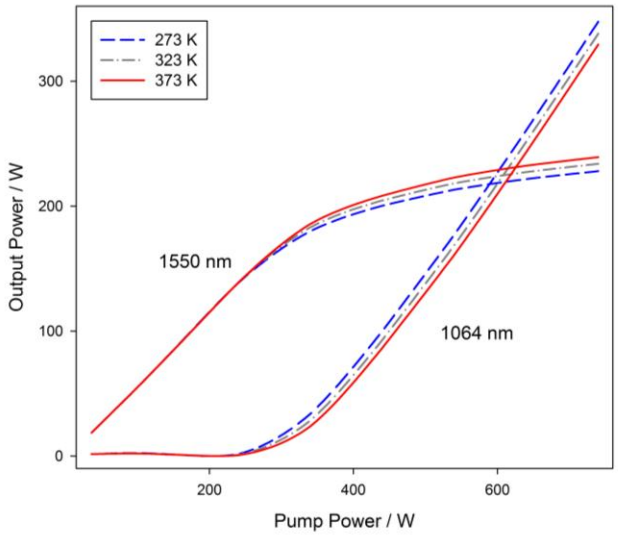

Figure 8. Output power at 1.5 μm and 1.0 μm as a function of pump power at different environmental temperatures.

3.2. Fiber optimization

We also investigate the effect of doping concentrations of Er^{3+}-ions and Yb^{3+}-ions on the output power at 1.5 μm and 1.0 μm. The modeling results exemplified in Fig. 9 show that increasing the doping concentrations of Er^{3+}-ions and Yb^{3+}-ions is beneficial to improve the 1.5 μm output and suppress the 1.0 μm output. It is worth mentioning that we do not take the clustering effect into consideration. In practice, increasing the doping concentrations of Er^{3+}-ions may result in clustering effect which could significantly degrade the conversion efficiency [9].

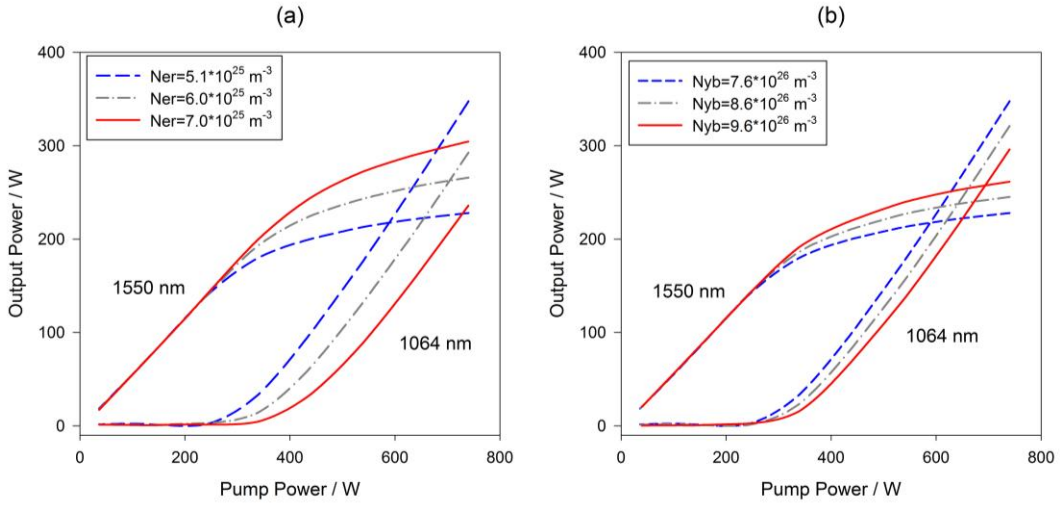

Figure 9. (a) Output power at 1.5 μm and 1.0 μm as a function of pump power at different doping concentrations of Er^{3+}-ions. (b) Output power at 1.5 μm and 1.0 μm as a function of pump power at different doping concentrations of Yb^{3+}-ions.

Effect of reflection at fiber ends is also investigated. As illustrated in Fig. 10 that to get the maximum 1.5 μm output and minimum 1.0 μm, we can reduce the reflectivities at both fiber ends. It means that in practice, to get a larger 1.5 μm output, we can simply angle-cleave the fiber ends instead of perpendicularly-cleave.

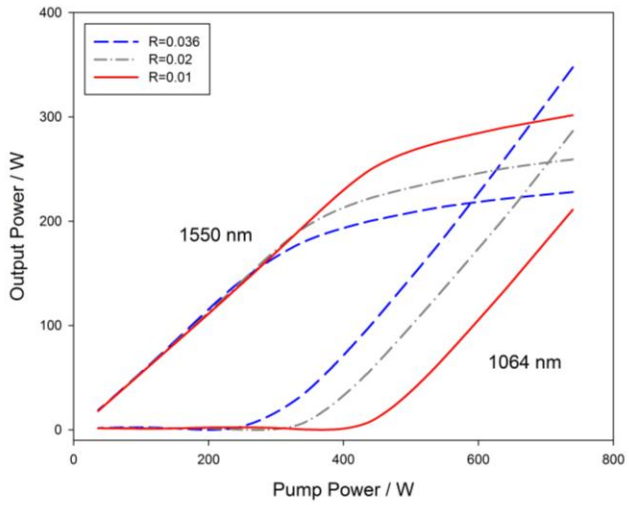

Figure 10. Output power at 1.5 μm and 1.0 μm as a function of reflectivity at fiber ends.

4. CONCLUSION

Effect of the fiber temperature on lasing performance is investigated in high-power, cladding-pumped, double-clad Er, Yb co-doped fiber laser system. The temperature profile in the fiber is sketched with the consideration of quantum defect heat, heat from the absorption of spontaneous emission, and the convection and radiation at the heat transfer boundaries. It is showed that increasing the fiber's temperature is an effective strategy to suppress 1 μm parasitic lasing and improve the lasing performance at 1.5 μm, a similar phenomenon is found with enhancing doping concentrations of the two ions and decreasing the reflectivities at the fiber ends.

ACKNOWLEDGEMENT

The works is supported by the National Natural Science Foundation of China (NSFC 61078035, 61177045), the Research Fund for the Doctoral Program of Higher Education of China (RFDP: 20110071110016) and the Priority Academic Program Development of Jiangsu Higher Education Institutions (PAPD).We also thank the support from the Innovation Research Fund for Excellent Graduate Students (No.EZH1232317) from Fudan University to the first author.

REFERENCES

[1] E. Yahel, and A. Hardy, "Modeling high-power Er^{3+}-Yb^{3+} codoped fiber lasers," Journal of lightwave technology, 21(9), 2044 (2003).
[2] G. A. Sefler, W. D. Mack, G. C. Valley *et al.*, "Secondary energy transfer and nonparticipatory Yb^{3+}ions in Er^{3+}-Yb^{3+} high-power amplifier fibers," JOSA B, 21(10), 1740-1748 (2004).
[3] M. Karasek, "Optimum design of Er^{3+}-Yb^{3+} codoped fibers for large-signal high-pump-power applications," IEEE Journal of Quantum Electronics, 33(10), 1699-1705 (1997).
[4] Q. Han, J. Ning, and Z. Sheng, "Numerical investigation of the ASE and power scaling of cladding-pumped Er–Yb codoped fiber amplifiers," IEEE Journal of Quantum Electronics, 46(11), 1535-1541 (2010).
[5] V. Gainov, R. Shaidullin, and O. A. Ryabushkin, "Steady-state heating of active fibres under optical pumping," Quantum Electronics, 41(7), 637 (2011).
[6] P. Yan, A. Xu, and M. Gong, "Numerical analysis of temperature distributions in Yb-doped double-clad fiber lasers with consideration of radiative heat transfer," Optical Engineering, 45(12), 1242011-1242014 (2006).
[7] D. E. McCumber, "Theory of Phonon-Terminated Optical Masers," Physical review, 134(2A), A299-A306 (1964).
[8] Y. Jeong, S. Yoo, C. Coderaard *et al.*, "Erbium: ytterbium codoped large-core fiber laser with 297-W continuous-wave output power," IEEE Journal of Selected Topics in Quantum Electronics, 13(3), 573-579 (2007).
[9] G. C. Valley, "Modeling cladding-pumped Er/Yb fiber amplifiers," Optical Fiber Technology, 7(1), 21-44 (2001).